Merged Beam Studies of Associative Ionization

A. Le Padellec[1], X. Urbain[2], T. Nzeyimana[2] and E.A. Naji[2]
[1]LCAR UMR 5589 - Université Paul Sabatier-Toulouse III - 118, Route de Narbonne Bât. IIIR1b4 31062 Toulouse Cedex 4, France; [2]Unité FYAM - Département de Physique - Université Catholique de Louvain (LLN) - Chemin du cyclotron 2 - B-1348 Louvain la Neuve, Belgium
lepadellec@yosemite.ups-tlse.fr, urbain@fyam.ucl.ac.be

1. INTRODUCTION

Carbon monoxide was detected in emission in the supernova 1987A spectrum and it is likely that its ion, CO^+, has also been detected.[1] The radiative association process was considered[2] for formation of CO^+, from $C^+ + O$, but not the associative ionization (AI) process from charged reactants $C^+ + O^-$. Bertrand and Van Tiggelen[3] found that the process, $N(^2D, ^2P)+O(^3P)\rightarrow NO^+ +e$, is the primary source of nitrogen oxide cations in ammonia and hydrogen-oxygen-nitrogen flames. The AI process that arises from the charged reactants $N^+ + O^-$, was not considered. The hydroxyl cation, OH^+, was detected in interstellar clouds[4] (where its destruction leads to H_3O^+), in comets and in planetary atmospheres[5]. It is important to characterize the formation pathways for OH^+, and among them the AI process. Here, we provide AI cross sections for the association of charged reactants that leads to the production of CO^+, NO^+, O_2^+ and OD^+.

2. EXPERIMENTAL TECHNIQUE

The whole apparatus can be divided into four sections pumped at ultra high vacuum. The first one includes the ion sources, the acceleration, and the mass selectors as well as the beam optics. In the second section, the two ionic beams are merged. The third section has the 7.8 cm (length)

interaction region. The last section contains the magnetic analyzer where the intensities of the primary beams as well as that of the reaction products are recorded. In a merged beam set-up, the number of reactions, N, that occur within a certain time, T, is connected to the absolute cross section σ by the following expression:

$$N(T)=\sigma\frac{v_r}{q_1 q_2 v_1 v_2}F\int_0^T I_1(t)I_2(t)dt \quad (1)$$

where v_r, v_1, v_2, q_1, q_2, I_1 and I_2 depict the relative velocity, the laboratory velocities of the two beams, their charges and their intensities, respectively. The form factor, F, is assumed to be time independent. It is a non-trivial parameter to establish, since it involves the measurement of the density profiles of the two interacting beams. However, one can overcome this experimental difficulty. Indeed, if the two beams display a sharply characterized cross section but also a perfect overlap over a known region L, the form factor would be simply expressed by:

$$F=\frac{L}{S_>} \quad (2)$$

where $S_>$ denotes the section of the largest beam. In practice, one only needs to strongly diaphragm the two beams just before they interact and make use of the cores of the two reactant beams. L is defined cautiously, by applying a certain observation voltage, V, in the interaction region. The molecular cations formed in this region experience an increase of their kinetic energy by an amount +eV and are therefore completely distinguishable, after magnetic analysis, from other molecular cations produced anywhere else. The interaction length is therefore equal to that of the region where the electric potential is equal to V. The kinematics of the merged beam experiment give the center-of-mass energy, E_{cm}, as

$$E_{cm}=\mu\left[\sqrt{\frac{q_2(A_2-V)}{m_2}}-\sqrt{\frac{q_1(A_1-V)}{m_1}}\right] \quad (3)$$

with μ, A_1, A_2, m_1 and m_2, the reduced mass, accelerating voltages and masses, respectively. Thus, a fine adjustment of the center of mass energy can be achieved while changing the observation voltage. Cross sections are measurable down to 10meV.

The C^+, N^+, O^+ and D^+ beams were produced within the ECR ion source,

located about 2.6 m upstream to the interaction region, whereas the anionic beams O^- and D^- were produced within a duoplasmatron ion source. The electronic excitation of the O^- and D^- target beams is not a problem since they display a unique stable electronic level. However, the excitation of the cationic counterparts is far from being simple. For C^+ below 10 eV, in addition to the ^2P ground state, there are two excited states, the ^4P and ^2D lying at 5.33 and 9.29 eV, respectively. For N^+ below 6 eV, there are three states above the ^3P ground state, the ^1D, ^1S and ^5S at 1.90, 4.05 and 5.85 eV, respectively. For O^+ below 6 eV, there are two states above the ^4S ground state, namely the ^2D and ^2P at 3.32 and 5.02 eV, respectively. Evidence of metastable contamination was demonstrated by Harrison et al.[6] in their N^+ ion beam, in particular with the ^1D and ^1S states. Moreover, the presence of electronically excited cations N^+ and O^+ was explicitly highlighted by Hamdan and Brenton[7] on one hand, and by Reid[8] on the other hand, who show that about 45 % of the O^+ cations produced by electron impact of O_2 were in the ^2P and ^2D metastable states. It is necessary to evaluate the residence time of the cations within the ECR source plus their time-of-flight and compare these with the different possible transition lifetimes of the cations.

The residence times are about 1.4, 2.0 and 2.1 μs, for C^+, N^+ and O^+, respectively. The time-of-flights are 8.4, 8.7 and 9.3μs, respectively.

For the C^+ cations, the radiative lifetimes for the $^2D \rightarrow ^2P$ and $^4P \rightarrow ^2P$ transitions, are 3.5 ns and at least 6.7 ms, respectively. Therefore, the ^2D state had time to decay, and the C^+ beam was comprised of a mixture $C^+(^2P$ and $^4P)$. For the N^+ cations, the lifetimes for the $^1S \rightarrow ^1D$ and $^1D \rightarrow ^3P$ transitions, are 855ms and 275s, respectively. If produced, the ^1S and ^1D states of the target N^+ ions are populated, in addition to the ^3P ground state. For the O^+ $^2P \rightarrow ^4S$ and $^2D \rightarrow ^4S$ transitions, the lifetimes are at least 19 and 6290 s, respectively. The ^2D and ^4S states are populated in the interaction region.

The energy resolution is an important issue, especially for the low center-of-mass energy data that we will present below. The AI process from charged particles is, indeed, a pure Coulomb interaction case for which the cross section should behave like E_{cm}^{-1} in the low energy limit. Together with each set of our low energy cross section data, we display this E_{cm}^{-1} dependence, folded with our experimental energy resolution.

3. EXPERIMENTAL RESULTS

3.1 $C^+ + O^-$

The AI cross sections are in Fig. 1a. The full line below 1 eV fits our data. extremely well. At low CM energy, the AI process populates rovibrational levels of several electronic states of CO^+: X $^2\Sigma^+$, A $^2\Pi$ and B $^2\Sigma^+$. Therefore, this measurement refers to total AI cross sections. It is difficult to give a qualitative and quantitative description of the AI process due to the scarcity of the relevant molecular data. Indeed, the correlation rules gives twelve states that correlate to the $C^+(^2P) + O^-(^2P)$ limit. These are $^{1,3}\Sigma^+(2)$, $^{1,3}\Sigma^-(1)$, $^{1,3}\Pi(2)$, and $^{1,3}\Delta(1)$, all poorly documented. The numbers in parentheses represent the number of electronic states of that particular symmetry. Depending upon the CM energy of the $C^+ + O^-$ system, several channels are open in the studied energy range (<20 eV):

$$
\begin{aligned}
C^+(^2P) + O^-(^2P) &\rightarrow CO(X^1\Sigma^+) + 20.89\text{eV} \\
&\rightarrow C(^3P) + O(^3P) + 9.80\text{eV} \\
&\rightarrow CO^+(X^2\Sigma^+) + e + 6.88\text{eV} \\
&\rightarrow C^+(^2P) + O(^3P) + e - 1.46\text{eV} \\
&\rightarrow C(^3P) + O^+(^4S) + e - 3.82\text{eV} \\
&\rightarrow C^+(^2P) + O^+(^4S) + 2e - 15.08\text{eV} \\
&\rightarrow CO^{2+}(X^3\Pi) + 2e - 20.38\text{eV}
\end{aligned}
$$

One might expect an interplay between AI and the four endothermic processes. Below about 1 eV, only a structureless E^{-1} dependence can be seen in Fig. 1a. The opening of the $C^+(^2P) + O(^3P) + e$ channel, i.e. collisional detachment, nearly coincides with the rapid fall-off of our measured cross sections above 2.5 eV. For higher energies, the cross sections decrease to a non-measurable level just below 15 eV where abruptly decrease again. This may be due to the opening of the $C^+(^2P) + O^+(^4S) + 2e$ channel to which $CO^{2+}(X\ ^3\Pi)$ correlates.

3.2 $N^+ + O^-$

The AI cross sections are in Fig. 1b. The line below 1 eV represents the E_{cm}^{-1} dependence and again, the model fits reasonably well. Several electronic states and rovibrational levels of NO^+ can be populated : $X^1\Sigma^+$, $a^3\Sigma^+$, $b^3\Pi$, $w^3\Delta$, $b'^3\Sigma^-$, $A'^1\Sigma^-$, $w^1\Delta$ and $A^1\Pi$. Once again there is a paucity of molecular

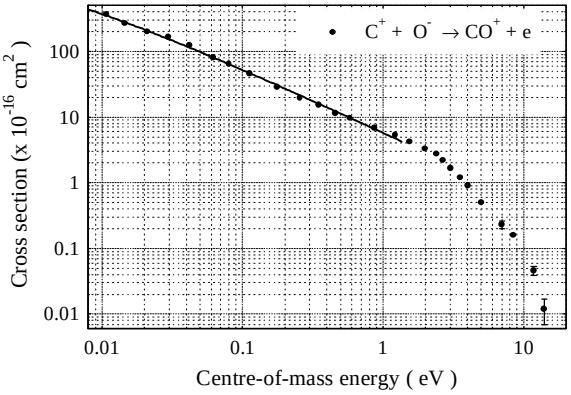

Figure 1a. The filled circles represent the AI cross sections for $C^+ + O^-$ whereas the full line shows the normalized data with the 1/E dependence.

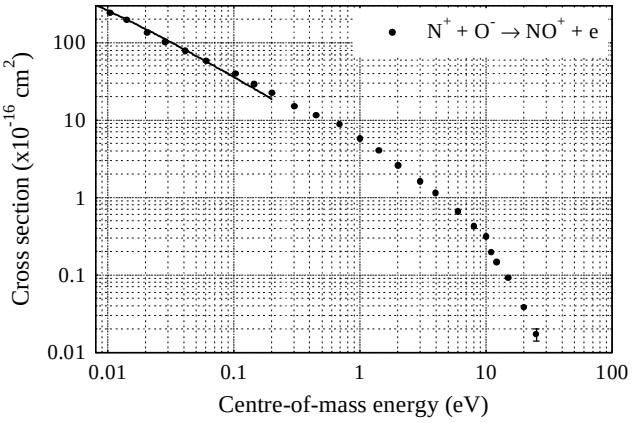

Figure 1b. The filled circles represent the AI cross sections for $N^+ + O^-$ whereas the full shows the normalized data with the 1/E dependence.

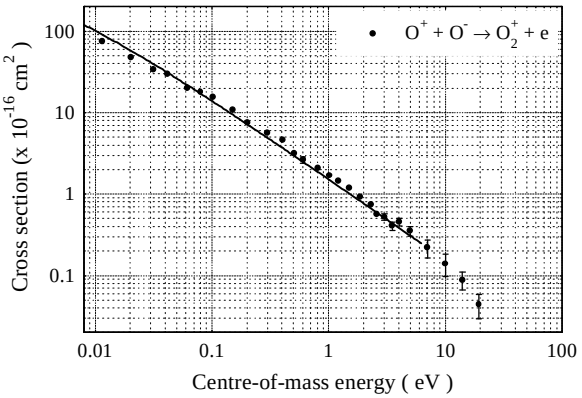

Figure 1c. The filled circles represent the AI cross sections for $O^+ + O^-$ whereas the full line shows the normalized data with the 1/E dependence.

data. We know from the correlation rules that twelve states correlate to the lowest $N^+(^3P) + O^-(^2P)$ limit and most are not characterized. These are the $^{2,4}\Sigma^+(1)$, $^{2,4}\Sigma^-(2)$, $^{2,4}\Pi(2)$, and $^{2,4}\Delta(1)$ states. For the next limit, $N^+(^1D) + O^-(^2P)$, there are nine states: $^2\Sigma^+(2)$, $^2\Sigma^-(1)$, $^2\Pi(3)$, $^2\Delta(2)$, and $^2\Phi(1)$. Depending upon the CM energy of $N^+ + O^-$, several channels are open over the studied energy range (<30 eV):

$$
\begin{aligned}
N^+(^3P) + O^-(^2P) &\rightarrow NO(X^2\Pi_r) + 19.55\text{eV} \\
&\rightarrow N(^4S) + O(^3P) + 13.07\text{eV} \\
&\rightarrow NO^+(X^1\Sigma^+) + e + 10.29\text{eV} \\
&\rightarrow N(^4S) + O^+(^4S) + e - 0.54\text{eV} \\
&\rightarrow N^+(^3P) + O(^3P) + e - 1.46\text{eV} \\
&\rightarrow N^+(^3P) + O^+(^4S) + 2e - 15.07\text{eV} \\
&\rightarrow NO^{2+}(X^2\Sigma^+) + 2e - 18.85\text{eV}
\end{aligned}
$$

AI and the four endothermic processes that can all interact with each other, have never been the subject of any reported work. Below about 0.7 eV, only a structureless E^{-1} energy dependence can be seen in Fig. 1b. At 0.54eV, it is difficult to relate the opening of $N(^4S) + O^+(^4S) + e$ to any structure in the AI curve. This is expected since it would correspond to a transfer ionization process in which the oxygen anion would lose two electrons. Moreover, the rapid fall-off that we observe above 6 eV does not seem to coincide with the opening of the $N^+(^3P) + O(^3P) + e$ channel, which lies at 1.46 eV. At higher energies, the cross sections decrease to a non-measurable level just below 20 eV. This may be caused by the opening of the $N^+(^3P) + O^+(^4S) + 2e$ channel to which the $NO^{2+}(X^2\Sigma^+)$ correlates.

3.3 $O^+ + O^-$

The AI process originating from $O^+ + O^-$ is presented in Fig. 1c. At low cm energies, three electronic states of the O_2^+ ions can be populated: $X^2\Pi$, $a^4\Pi_u$ and $A^2\Pi_u$. Excited states such $b'^4\Pi_g$, $b^4\Sigma_g^-$ and $C^2\Phi_u$, may be populated as well. According to the correlation rules, the $^{3,5}\Sigma^+_{u,g}(1)$ and $^{3,5}\Pi_{u,g}(1)$ states correlate to the ground state $O^+(^4S) + O^-(^2P)$ limit. Moreover, thirty six states, $^{3,5}\Sigma^+_{u,g}(2)$, $^{3,5}\Sigma^-_{u,g}(1)$, $^{3,5}\Pi_{u,g}(3)$, $^{3,5}\Delta_{u,g}(2)$ and $^{3,5}\Phi_{u,g}(1)$, correlate to the next limit, $O^+(^2D) + O^-(^2P)$. Depending upon the CM energy, several channels are open (at <20 eV):

$$
\begin{aligned}
O^+(^4S) + O^-(^2P) &\rightarrow O_2(X^3\Sigma_g^-) + 17.27eV \\
&\rightarrow O(^3P) + O(^3P) + 12.15eV \\
&\rightarrow O_2^+(X^2\Pi_g) + e + 5.20eV \\
&\rightarrow O(^3P) + O^+(^4S) + e - 1.46eV \\
&\rightarrow O^+(^4S) + O^+(^4S) + 2e - 15.07eV \\
&\rightarrow O_2^{2+}(X^1\Sigma_g^+) + 2e - 18.65eV
\end{aligned}
$$

On purely energetic grounds, there should be interplay between the AI and the three endothermic processes at large CM energies. It is remarkable that below 7 eV, only a structureless E^{-1} energy dependence can be seen in Fig. 1c, and that the opening of the $O(^3P) + O^+(^4S) + e$ channel that occurs at 1.46 eV, does not give rise to any structure in the cross section curve. On the other hand, the shallow fall off above 10 eV might be caused by the opening of the $O^+(^4S) + O^+(^4S) + 2e$ channel to which the $O_2^{2+}(X\ ^1\Sigma_g^+)$ correlates.

3.4 $O^+ + D^-$ and $D^+ + O^-$

The AI cross section are in Fig. 2. The low energy dependence for the $O^+ + D^-$ channel is remarkable because it does not follow the E_{cm}^{-1} law. This is not due to an experimental artifact but rather to a not yet elucidated physical effect. Few electronic states of the OD^+ ions can be populated : $X\ ^3\Sigma^-$, a $^1\Delta$, b $^1\Sigma^+$ and $A^3\Pi$ states. The paucity of the molecular data is once again a problem and is surprising since the hydroxyl cation is quite well documented.

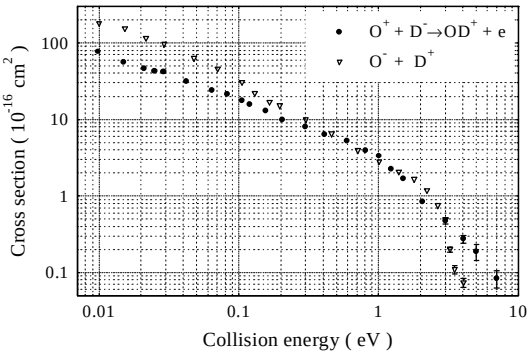

Figure 2. The open triangles represent the AI cross sections for $D^+ + O^-$ and the filled circles represent the data for $O^+ + D^-$.

We know from the correlation rules that two states arise from the $D^+ + O^-(^2P)$ limit and to the best of our knowledge, they are not characterized. These are the $^2\Sigma^+(1)$ and $^2\Pi(1)$ states. From the three $O^+(^4S, ^2D, ^2P) + D^-(^1S)$ limits, six states arise: $^4\Sigma^-(1)$, $^2\Sigma^-(1)$, $^2\Pi(1)$, $^2\Delta(1)$, $^2\Sigma^+(1)$ and $^2\Pi(1)$. The first state is from $O^+(^4S)$. The next three are from $O^+(^2D)$ and the last two are from $O^+(^2P)$.

Depending upon the center-of-mass energy in the $D^+ + O^-$ and $O^+ + D^-$ systems, several channels are open over the studied energy range (<10 eV):

$O^-(^2P) + D^+$	$\rightarrow OD(X^2\Pi) + 16.53$ eV
	$\rightarrow O(^3P) + D(^2S) + 12.14$ eV
	$\rightarrow OD^+(X^3\Sigma^-) + 3.51$ eV
	$\rightarrow O^+(^4S) + D^-(^1S) - 0.72$ eV
	$\rightarrow O(^3P) + D^+ - 1.46$ eV
	$\rightarrow O^+(^4S) + D(^2S) - 1.48$ eV
	$\rightarrow O^+(^4S) + D^+ - 15.08$ eV
$O^+(^4S) + D^-(^1S)$	$\rightarrow OD(X^2\Pi) + 17.25$ eV
	$\rightarrow O(^3P) + D(^2S) + 12.86$ eV
	$\rightarrow OD^+(X^3\Sigma^-) + 4.23$ eV
	$\rightarrow O^-(^2P) + D^+ + 0.72$ eV
	$\rightarrow O(^3P) + D^+ - 0.74$ eV
	$\rightarrow O^+(^4S) + D(^2S) - 0.76$ eV
	$\rightarrow O^+(^4S) + D^+ - 14.36$ eV

Concerning the interplay between the processes at higher energies, the opening up of the $O(^3P)+D^++e$ and $O^+(^4S)+D(^2S)+e$ channels affect the $O^+ + D^-$ AI curve whereas the $O^+(^4S)+D^++2e$ channel does not play any role (where AI is already at a non-measurable level). The $O^+(^4S)+D^-(^1S)$ channel does not affect $D^+ + O^-$ AI whereas the AI cross section is affected by the $O(^3P)+D^++e$ and $O^+(^4S)+D(^2S)+e$ channels. The $O^+(^4S)+D^++2e$ does not play any role.

4. CONCLUSION

The cross sections for the AI processes (C^+, N^+, O^+ and D^+) + O^- and those for $O^+ + D^-$ were measured. Special attention was paid to the internal energy of the target cation. Our most important result concerns the large size of the measured cross sections, which reach values near $1x10^{-14}$ cm^2 at thermal energies. The lack of molecular data is a limiting factor in formulating qualitative and quantitative interpretations.

REFERENCES

1 P. Bouchet, E. Slezak, T. LeBertre, A. Moneti and J. Manfroid, A. & A. **80**, 379 (1989).
2 A. Dalgarno, M. L. Du and J. H. You, Astrophys. J. **349**, 675 (1990).
3 C. Bertrand and P. J. van Tiggelen, J. Phys. Chem. **78**, 2320 (1974).
4 M. A. Coplan, K. W. Olgilvie, M. F. A'Heare, P. Boschler and J. Geiss, J. Geosphys. Res. **92**, 39 (1987).
5 W. F. Huebner in The Photochemistry of Atmospheres, ed. by J.S. Levine (Academic Press, Orlando, 1985).
6 M. F. A. Harrison, K. Dolder and P. C. Thonemann, Proc. Phys. Soc. **82**, 368 (1963).
7 M. Hamdan and A. G. Brenton, J. Phys. B **22**, 2289 (1989).
8 C. J. Reid, J. Phys. B **25**, 475 (1992).